Variance reduction in computations of neoclassical transport in stellarators using a δf method

K. Allmaier,[1] S. V. Kasilov,[2] W. Kernbichler,[1] and G. O. Leitold[1]
[1]*Association EURATOM-ÖAW, Institut für Theoretische Physik-Computational Physics, Technische Universität Graz, Petersgasse 16, A-8010 Graz, Austria*
[2]*Institute of Plasma Physics, National Science Center "Kharkov Institute of Physics and Technology," Akademicheskaya str. 1, 61108 Kharkov, Ukraine*

(Received 28 December 2007; accepted 10 April 2008; published online 18 July 2008)

An improved δf Monte Carlo method for the computation of neoclassical transport coefficients in stellarators is presented. Compared to the standard δf method without filtering, the computing time needed for the same statistical error decreases by a factor proportional to the mean free path to the power 3/2. © *2008 American Institute of Physics*. [DOI: 10.1063/1.2918659]

I. INTRODUCTION

Various δf Monte Carlo methods are successfully used for modeling of neoclassical transport in tokamaks and stellarators.[1–5] These methods solve the linearized drift-kinetic equation taking into account the source term in the equation for test particle weights which evolve with time. The original δf method[1] for the computation of transport coefficients, which is named below "standard δf method," has a good convergence for tokamaks where the variance of all transport coefficients including the bootstrap coefficient has no strong dependence on plasma collisionality. However, in stellarators, the variance of the bootstrap coefficient increases for this method as a square of the mean free path due to the accumulation of large random contributions to the test particle weights which occurs in the phase space region occupied by trapped particles. The test particle weight in the standard δf method coincides with test particle displacement from the original magnetic surface where transport coefficients are computed and particles with large weights correspond to trapped particles which have a finite bounce averaged radial drift velocity and, therefore, can make large radial displacements in the long mean free path regime. In order to overcome the problem of large noise in the bootstrap coefficient it has been proposed in Ref. 5 to filter out particles which acquire large weights replacing them by particles with zero weight, i.e., put the particles with large deviations from the magnetic surface back to this original surface (as it is also done in the original method[1]) limiting the radial size of the annulus where test particles can move by the width much smaller than the trapped particle displacement during a collision time. This procedure largely improves the convergence for computing the bootstrap coefficient but also introduces some bias in the result which must be checked additionally.

In Ref. 6 a method with reduced variance which combines the standard δf method with an algorithm employing constant particle weights and rediscretizations of the test particle distribution in phase space has been presented. This method is formally free of bias and allows simultaneous computations of bootstrap coefficient and diffusion coefficient (the latter possibility is destroyed by filtering). There, this method has been tested in confinement regimes with negligible radial electric field. In the present work this method is described in detail and results for general confinement regimes are presented for two stellarator configurations.

The structure of the paper is as follows: In Sec. II the standard δf method is formulated in the form of an integral equation. Being fully equivalent to the usual formulation of the δf Monte Carlo method, the integral formulation allows a direct use of various variance reduction methods which are usually introduced for integral equations. In Sec. III a modified δf method is described and it is illustrated with the numerical results for two modern stellarators in Sec. IV. A short summary of the results is given in Sec. V.

II. δF METHOD

A. Basic equations

Monoenergetic transport coefficients are determined by the steady state solution of the linearized drift kinetic equation for the normalized perturbation of the distribution function $\hat{f}$ (which is also named "marker"). If the total energy and the perpendicular adiabatic invariant are used as velocity space variables this equation takes the following form:

$$\mathcal{L}_D\hat{f} \equiv \left(\frac{\partial}{\partial t} + \mathbf{V}_g \cdot \nabla - \mathcal{L}_C\right)\hat{f} = \dot{\psi} \equiv \mathbf{V}_g \cdot \nabla\psi, \tag{1}$$

where $\mathbf{V}_g$ and $\dot{\psi}$ are guiding center drift velocity and its contravariant ψ-component, respectively, ψ is a flux surface label, $\mathcal{L}_C$ is the Lorentz collision operator, and the marker $\hat{f}$ is defined through the local Maxwellian distribution function f_M and the total distribution function f via

$$f = f_M - \hat{f}\frac{\partial f_M}{\partial \psi}. \tag{2}$$

In the following it is convenient to use instead of the total energy and the perpendicular invariant the velocity module v and the pitch parameter $\lambda = v_\parallel / v$ as velocity space variables. In these variables the collision operator is given as

$$\mathcal{L}_C = \frac{v}{l_c}\frac{\partial}{\partial\lambda}(1-\lambda^2)\frac{\partial}{\partial\lambda}, \tag{3}$$

where l_c is the mean free path, and the monoenergetic radial diffusion coefficient and the normalized bootstrap coefficient, respectively, are given by

$$D_{\mathrm{mono}} = -\frac{1}{\langle|\nabla\psi|\rangle^2}\left\langle\frac{1}{2}\int_{-1}^{1}\mathrm{d}\lambda\hat{f}\dot{\psi}\right\rangle, \tag{4}$$

$$\lambda_{bb} = -\frac{3}{\rho_L B_0\langle|\nabla\psi|\rangle}\left\langle\frac{1}{2}\int_{-1}^{1}\mathrm{d}\lambda\hat{f}\lambda B\right\rangle. \tag{5}$$

Here, ρ_L is the Larmor radius in the reference magnetic field B_0, B is the magnetic field module, and

$$\langle A\rangle = \frac{\int\mathrm{d}\vartheta\int\mathrm{d}\varphi\sqrt{g}A}{\int\mathrm{d}\vartheta\int\mathrm{d}\varphi\sqrt{g}} \tag{6}$$

denotes the average over the volume between neighboring flux surfaces with ϑ and φ being the poloidal and the toroidal angles of flux coordinates and g is the metric determinant of flux coordinates (ψ,ϑ,φ). In the absence of a temperature gradient and a radial electric field the quantity λ_{bb} is linked to the equilibrium (bootstrap) current density $j_\parallel$ and the gradient of the pressure p by

$$\lambda_{bb} = -\langle j_\parallel B\rangle\left(c\langle|\nabla\psi|\rangle\frac{\mathrm{d}p}{\mathrm{d}\psi}\right)^{-1} \tag{7}$$

if l_c is put to a constant during the energy convolution. In the following D_{mono} is normalized by the plateau diffusion coefficient

$$D_{\mathrm{plateau}} = \frac{\pi v\rho_L^2}{8\sqrt{2}\iota R}, \tag{8}$$

where ι is the rotational transform and R is the major radius.

It should be noted that the drift motion of test particles is described exactly by the operator $\mathcal{L}_D$ (which includes also the radial motion) in Eq. (1). As a result, $\mathcal{L}_D$ conserves the total energy but not the kinetic energy alone. Therefore, strictly speaking, $\hat{f}$ is not monoenergetic if a radial electric field is present. However, the typical change of the kinetic energy of the test particle during a couple of collision times needed to model $\hat{f}$ is small compared to the original test particle energy if the amplitude of the magnetic field modulation on the magnetic surface is small (a usual argument justifying the monoenergetic approach). Therefore this change of the kinetic energy of test particles is ignored in the following and v is treated there as a parameter but not as an independent phase space coordinate. Also, the local approach of neoclassical theory assumes that change of the radial variable ψ during test particle motion is negligibly small and, therefore, ψ plays the role of a parameter. This limit can be realized with any accuracy by scaling both, the magnetic field and radial electric field with the same sufficiently large factor. Thus, despite the fact that test particle trajectories are integrated in the full $(\psi,\vartheta,\varphi,v,\lambda)$ phase space, the dependence of the perturbed distribution function $\hat{f}$ on ψ and v is treated as parametric and the set of independent variables $\mathbf{z}$ is reduced to $(\vartheta,\varphi,\lambda)$ for the solutions of kinetic Eq. (1) in the following.

B. Integral formulation of the Monte Carlo procedure

Traditionally,[7] the Monte Carlo procedure for the solution of the drift kinetic equation is introduced directly for Eq. (1) by defining a random step over test particle phase space coordinates for a small time interval Δt and by verifying that the Fokker–Planck equation describing test particle orbits advanced by such steps coincides with the original drift kinetic equation. At the same time, a variety of variance reduction methods developed mainly for Monte Carlo solutions of integral equations need some reformulation in order to develop an algorithm. In order to enable a direct use of these methods, it is convenient to rewrite Eq. (1) in the integral form using a Green's function G defined by

$$\mathcal{L}_D G(t,\mathbf{z},\mathbf{z}_0) = 0, \tag{9}$$

$$G(0,\mathbf{z},\mathbf{z}_0) = [g(\mathbf{z}_0)]^{-1/2}\delta(\mathbf{z}-\mathbf{z}_0), \tag{10}$$

where $\mathbf{z}=(\vartheta,\varphi,\lambda)$. This Green's function is normalized to 1,

$$\int \mathrm{d}^3z[g(\mathbf{z})]^{1/2}G(t,\mathbf{z},\mathbf{z}_0) = 1. \tag{11}$$

Thus, a formal solution to Eq. (1) is

$$\hat{f}(t,\mathbf{z}) = \int \mathrm{d}^3z_0[g(\mathbf{z}_0)]^{1/2}\left[G(t-t_0,\mathbf{z},\mathbf{z}_0)\hat{f}(t_0,\mathbf{z}_0) + \int_{t_0}^{t}\mathrm{d}t' G(t-t',\mathbf{z},\mathbf{z}_0)\dot{\psi}(\mathbf{z}_0)\right]. \tag{12}$$

If a steady state solution is looked for, $\hat{f}(t,\mathbf{z})=\hat{f}(\mathbf{z})$, Eq. (12) becomes an integral equation for $F(\mathbf{z})=[g(\mathbf{z})]^{1/2}\hat{f}(\mathbf{z})$ which is given below also in operator form,

$$F(\mathbf{z}) = \int \mathrm{d}^3z_0 K(\mathbf{z},\mathbf{z}_0)F(\mathbf{z}_0) + Q(\mathbf{z}) \equiv \mathcal{K}F + Q, \tag{13}$$

where

$$K(\mathbf{z},\mathbf{z}_0) = [g(\mathbf{z})]^{1/2}G(\Delta t,\mathbf{z},\mathbf{z}_0), \tag{14}$$

Δt is the integration time step, and

$$\begin{aligned} Q(\mathbf{z}) &= \int \mathrm{d}^3z_0[g(\mathbf{z})g(\mathbf{z}_0)]^{1/2}\int_0^{\Delta t}\mathrm{d}t' G(t',\mathbf{z},\mathbf{z}_0)\dot{\psi}(\mathbf{z}_0) \\ &\equiv [g(\mathbf{z})]^{1/2}\Delta\psi(\mathbf{z}) \\ &\approx [g(\mathbf{z})]^{1/2}\dot{\psi}(\mathbf{z})\Delta t. \end{aligned} \tag{15}$$

The Monte Carlo operator, $\mathbf{Z}(\Delta t,\mathbf{z}_0)$, is introduced as a random position of a test particle starting at $\mathbf{z}_0$ after a single time step modeled in a standard way.[7] First, the particle pitch is changed randomly in accordance with $\mathcal{L}_C$,

$$\lambda' = \lambda_0(1-\Delta_C) + [\Delta_C(1-\lambda_0^2)]^{1/2}\xi, \quad \Delta_C = \frac{v\Delta t}{l_c}, \tag{16}$$

where ξ is a random number which takes the values ± 1 with equal probabilities, and then an integration step of particle drift equations over the time interval Δt is performed. Thus, the kernel of the integral equation is given by an expectation value,

$$K(\mathbf{z},\mathbf{z}_0) = \overline{\delta(\mathbf{z} - \mathbf{Z}(\Delta t,\mathbf{z}_0))}. \tag{17}$$

More precisely, Eq. (17) can be viewed as a definition of the random process $\mathbf{Z}(\Delta t,\mathbf{z}_0)$ via the transition probability density $K(\mathbf{z},\mathbf{z}_0)$ while the algorithm described in Eq. (16) defines a linear approximation in Δt of this random process. At this point, in addition to $\mathbf{Z}(\Delta t,\mathbf{z}_0)$, random numbers $\mathbf{z}_{(k)} \equiv (\vartheta_{(k)},\varphi_{(k)},\lambda_{(k)})$ where $k=0,1,2,\ldots$ are introduced via the recurrence relation (19) and the probability density (22). Various overlined quantities below are the expectation values with respect to these random numbers.

The solution of Eq. (13) by direct iterations can be presented as an expectation value of an integral along the stochastic orbit,

$$F = \sum_{k=0}^{\infty} \mathcal{K}^k Q = C_0 \sum_{k=0}^{\infty} \overline{w_{(0)}\delta(\mathbf{z} - \mathbf{z}_{(k)})}, \tag{18}$$

$$\mathbf{z}_{(k)} = \mathbf{Z}(\Delta t,\mathbf{z}_{(k-1)}), \tag{19}$$

$$w_{(0)} = \Delta\psi(\mathbf{z}_{(0)}), \tag{20}$$

where

$$C_0 = \int \mathrm{d}^3 z [g(\mathbf{z})]^{1/2}, \tag{21}$$

and the random starting point $\mathbf{z}_{(0)}$ is chosen with the probability density

$$\overline{\delta(\mathbf{z} - \mathbf{z}_{(0)})} = C_0^{-1}[g(\mathbf{z})]^{1/2}. \tag{22}$$

The averages (4) are given by expectation values as

$$D_{\mathrm{mono}} = -\frac{1}{\langle|\nabla\psi|\rangle^2} \sum_{k=0}^{\infty} \overline{w_{(0)}\dot{\psi}(\mathbf{z}_{(k)})}, \tag{23}$$

$$\lambda_{bb} = -\frac{3}{\rho_L B_0 \langle|\nabla\psi|\rangle} \sum_{k=0}^{\infty} \overline{w_{(0)}\lambda_{(k)} B(\mathbf{z}_{(k)})}. \tag{24}$$

When $k\Delta t$ exceeds a few collision times, the correlation between $\mathbf{z}_{(k)}$ and $w_{(0)}$ is lost and, therefore, such terms in Eqs. (23) and (24) tend to zero, e.g.,

$$\overline{w_{(0)}\dot{\psi}(\mathbf{z}_{(k)})} \to \overline{w_{(0)}}\,\overline{\dot{\psi}(\mathbf{z}_{(k)})} = 0, \tag{25}$$

because

$$\overline{\lambda_{(k)} B(\mathbf{z}_{(k)})} = \int \mathrm{d}^3 z [g(\mathbf{z})]^{1/2} \lambda B(\mathbf{z}) = 0,$$

$$\overline{\dot{\psi}(\mathbf{z}_{(k)})} = \int \mathrm{d}^3 z [g(\mathbf{z})]^{1/2} \dot{\psi}(\mathbf{z}) = 0, \tag{26}$$

due to Liouville's theorem. The same is true also for $\overline{w_{(0)}}$. Thus, a finite sum over k in Eqs. (23) and (24) is sufficient.

The method of constant test particle weights described by Eqs. (23) and (24) has rather low variance for computations of D_{mono}, however, variance of λ_{bb} has a very unfavorable scaling with collisionality. Indeed, only the orbits originating in the boundary layer located in the velocity space around the trapped-passing boundary λ_{t-p} which is determined by the absolute maximum of the magnetic field on the flux surface contribute to λ_{bb} [the boundary layer has the width $\Delta\lambda \sim (L_c/l_c)^{1/2}$, where $L_c = 2\pi R/\iota$ is the connection length]. This follows from the fact that the test particle weight $w_{(0)}$ depends on the coordinates of the starting point of the orbit but is independent of the sign of the starting pitch parameter $\lambda_{(0)}$. Noticeable contributions to λ_{bb} are produced by test particles only when they are traveling in the passing phase space region because in the trapped region rapid oscillations of the pitch parameter λ are compensated in the time integral Eq. (24). Test particles starting deeply in the trapped particle region produce almost no contribution to λ_{bb} because when they reach the passing region after many oscillations in the magnetic well, probabilities to be detrapped to the co-passing region with $\lambda > 0$ and to the counter-passing region with $\lambda < 0$ become weakly dependent on the starting point [and, therefore, on $w_{(0)}$] and are almost the same. Thus, contributions from such particles compensate for each other statistically. Similar compensation takes place also for particles starting deeply in the passing region because correlation between the sign of the pitch parameter and the starting position [and, therefore, the weight $w_{(0)}$] is quickly lost for them (after passing the distance $l \sim l_c^{1/3} L_c^{2/3} \ll l_c$) while the amounts of particles starting from the same spatial point with $\pm\lambda_{(0)}$ are the same on average. Therefore, in the long mean free path regime only trapped particles starting from the boundary layer whose detrapping probabilities essentially depend on the starting position and passing particles from this layer whose trapping probabilities also depend on the starting position can produce on average an essential contribution to λ_{bb} (see Fig. 1). Actually, this manifests the fact that asymmetry in the passing particle distribution function is driven by the asymmetry of the boundary condition for this function at the trapped-passing boundary. Note that the contribution of a particle from the boundary layer is $\Delta\lambda$ times smaller than of a normal passing particle because of a higher trapping probability. Therefore, the variance of λ_{bb} scales for this method as $(l_c/L_c)^2$ in the long mean free path regime.

C. Standard δf method

It should be noted that the distribution of the test particles at each step remains to be the equilibrium distribution,

$$\overline{\delta(\mathbf{z} - \mathbf{z}_{(k)})} = C_0^{-1}[g(\mathbf{z})]^{1/2}, \tag{27}$$

which is independent of the pitch parameter λ (dependence of the metric determinant g on the full set of phase space variables $\mathbf{z}$ is only formal here). Therefore, the correlation between any function of $\mathbf{z}_{(k)}$ and any other function of $\mathbf{z}_{(j)}$ depends only on the time interval needed for the test particle to travel from the point $\mathbf{z}_{(k)}$ to $\mathbf{z}_{(j)}$, i.e., on the difference $k-j$,

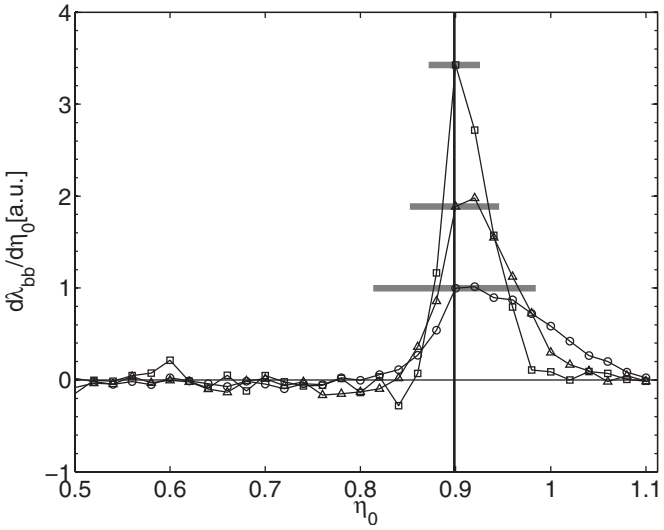

FIG. 1. Distribution $d\lambda_{bb}/d\eta_0$ of test particle contributions to λ_{bb} [Eq. (24)] over the starting values of the normalized perpendicular invariant $\eta_0=(1-\lambda_0^2)B_0/B(\mathbf{z}_0)$ for a tokamak with aspect ratio $R/r=10$, where B_0 is a reference magnetic field. Collisionality parameters L_c/l_c are 1×10^{-2} (○), 3×10^{-3} (△), and 1×10^{-3} (□). The width of the boundary layer for each curve is indicated by a horizontal bar. The position of the trapped-passing boundary is shown by the solid vertical line.

$$\overline{w_{(0)}\lambda_{(k-j)}B(\mathbf{z}_{(k-j)})}=\overline{w_{(j)}\lambda_{(k)}B(\mathbf{z}_{(k)})}, \tag{28}$$

where $w_{(j)}=\Delta\psi(\mathbf{z}_{(j)})\approx\dot{\psi}(\mathbf{z}_{(j)})\Delta t$. Thus the averages (23) and (24) can be presented as

$$D_{\mathrm{mono}}=-\frac{1}{\langle|\nabla\psi|\rangle^2}\lim_{k\to\infty}\overline{W_{(k)}\dot{\psi}(\mathbf{z}_{(k)})}, \tag{29}$$

$$=-\frac{1}{\langle|\nabla\psi|\rangle^2}\lim_{K\to\infty}\frac{1}{K}\sum_{k=0}^{K}\overline{W_{(k)}\dot{\psi}(\mathbf{z}_{(k)})}, \tag{30}$$

$$\lambda_{bb}=-\frac{3}{\rho_L B_0\langle|\nabla\psi|\rangle}\lim_{k\to\infty}\overline{W_{(k)}\lambda_{(k)}B(\mathbf{z}_{(k)})}, \tag{31}$$

$$=-\frac{3}{\rho_L B_0\langle|\nabla\psi|\rangle}\lim_{K\to\infty}\frac{1}{K}\sum_{k=0}^{K}\overline{W_{(k)}\lambda_{(k)}B(\mathbf{z}_{(k)})}, \tag{32}$$

where

$$W_{(k)}=\sum_{j=0}^{k}w_{(j)}=\psi(\mathbf{z}_{(k)})-\psi(\mathbf{z}_{(0)}) \tag{33}$$

is an integral of $\dot{\psi}$ along a stochastic orbit (total test particle displacement over ψ). The sum in Eq. (33) actually represents the integration formula which is linear in Δt for the linearized radial equation of motion [see the algorithm below Eq. (16), and the recurrence relation (19)]. For simplicity, the proof that $W_{(k)}$ corresponds to the radial displacement modeled exactly is omitted here in favor of the above argument. Nevertheless, in the computations $W_{(k)}$ is calculated integrating the radial equation of motion in the same manner as the rest of the drift equations, i.e., using a high order Runge–Kutta algorithm (see Sec. II A). Such a procedure of evaluating averages corresponds to a standard δf method.[1,4,5] For a tokamak, the variance of λ_{bb} for this method does not scale with the collisionality, and the required CPU time scales linearly with l_c/L_c. However, for stellarators the variance of λ_{bb} again recovers the scaling $(l_c/L_c)^2$ because due to the nonzero bounce-averaged drift of trapped particles large contributions to W_k are acquired, which scale as $\dot{\psi}l_c/v$. These contributions are weakly correlated with the values of $\lambda_{(k)}$ which test particles have after detrapping. This is due to the fact that detrapping probabilities to the co-passing and to the counter-passing phase space regions weakly depend on test particle position in the magnetic well and are almost equal as long as this particle is deeply trapped. Therefore, weight generated in the phase space regions of deeply trapped particles reaches co-passing or counter-passing phase space regions with almost equal probabilities and therefore on average is compensated statistically in λ_{bb}. Numerically this results in statistical compensation of large random numbers which introduces large variance in the computation. To overcome this problem in a standard δf method, the test particle motion is limited to an annulus, $\psi_0-\delta\psi<\psi<\psi_0+\delta\psi$, so that test particles which leave the annulus [particles with large $W_{(k)}$] are replaced with particles from the equilibrium distribution Eq. (27) with $W_{(k)}=0$ (new particles are placed at the middle of the annulus). This means that large weights are filtered out. In order to reduce the noise effectively, the size of this annulus, $\delta\psi$, should be small enough to avoid systematic errors (bias) in the result, and the annulus width should be larger than the particle displacement during a collision time. If the second condition is properly satisfied, practically no noise reduction for the bootstrap coefficient λ_{bb} will be achieved. If it is not satisfied, the simultaneously computed transport coefficient D_{mono} becomes biased, although for the computation of D_{mono} filtering would not be necessary at all. In Ref. 5 this condition has been violated for the sake of good convergence of the bootstrap coefficient where the bias still remained small. A procedure which is formally free of such bias and which does not need additional calculations for the control of the bias is therefore of interest.

III. VARIANCE REDUCTION

For a formally "unbiased" method it is convenient to split the source in Eq. (13) into "passing" and "trapped" sources $Q_p=\chi Q$ and $Q_t=Q-Q_p$ using

$$\chi=\frac{1}{2}\left[1+\tanh\left(\frac{|\lambda|-\lambda_{t-p}}{\Delta\lambda}\right)\right], \tag{34}$$

where λ_{t-p} is the pertinent trapped-passing boundary (see Fig. 2), and solve the problem with each source independently. Results for transport coefficients for these two sources are added up at the end. The problem with Q_p is solved with the standard method without using an annulus limiting the test particle motion. Since accumulation of large weights is avoided for this source, the convergence of the bootstrap coefficient is similar to that in a tokamak.

For the treatment of the problem with Q_t one should notice the following. In both formulas for the bootstrap coefficient, Eqs. (24) and (32), this coefficient is defined by a

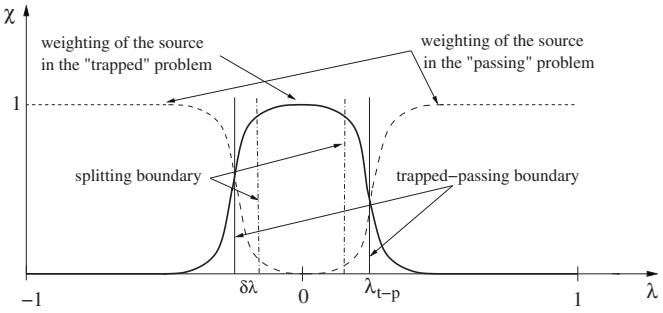

FIG. 2. Separation of the source in "trapped" and "passing" problems. The "splitting boundary" is located at a distance $\delta\lambda=2\Delta\lambda$ away from the trapped-passing boundary, where $\Delta\lambda$ is the width of the boundary layer.

time average of a test particle weight multiplied with λ. As long as a test particle is trapped it produces practically no contribution to λ_{bb} due to this averaging and the change of sign of λ at the reflection points. Therefore, trapped particles with large weights start to produce the noise in λ_{bb} only after detrapping. On the other hand, the total weight generated by Q_t in the phase space is zero. This is obvious in the case of stellarator symmetry because of $Q(-\mathbf{z})=-Q(\mathbf{z})$, but this is also true in a general case for the total source Q. In the general case the average of Q_t can be made zero also by redefining the function χ in terms of invariants of motion instead of λ. Particles with different signs of the weight detrapped from different magnetic wells quickly mix up in the close vicinity of the boundary layer so that each phase space volume element in this region contains both, particles with positive and negative weights if the number of test particles is large enough. The total weight in such a volume element which actually determines the distribution function being of relevance for the averages is smaller than the sum of the modulus of test particle weights contained in this element. Therefore a periodic rediscretization procedure which replaces all particles in the phase space volume element ("cell") with fewer particles with equal weights which carry the total weight in this element would lead to a significant reduction in the test particle number. It should be noted however, that the number of cells needed for rediscretization in the 3D phase space without significant bias from the finite size of the cells must be large and usually exceeds the number of test particles. Therefore, certain time averaging is needed for an effective rediscretization procedure. In order to introduce such a procedure, the formal solution to Eq. (13) can be presented as

$$F = F_M + \Delta F_M, \tag{35}$$

where F_M satisfies an equation which differs from Eq. (13) only by a source term,

$$F_M = \mathcal{K}F_M + Q_M, \tag{36}$$

where

$$Q_M = \frac{1}{M}\sum_{k=0}^{M-1} \mathcal{K}^k Q = Q_M(Q), \tag{37}$$

$$\Delta F_M = \sum_{k=0}^{M-1}\left(1-\frac{k+1}{M}\right)\mathcal{K}^k Q = \Delta F_M(Q). \tag{38}$$

For this purpose, the original equation (13) is transformed to

$$F = \sum_{k=0}^{m-1} \mathcal{K}^k Q + \mathcal{K}^m F, \tag{39}$$

where m is an arbitrary natural number. Averaging the r.h.s. of Eq. (39) over $1 \leqslant m \leqslant M$ yields

$$F = \Delta F_M + \frac{1}{M}\left(\sum_{m=0}^{M-1} \mathcal{K}^m Q + \sum_{m=1}^{M} \mathcal{K}^m F\right). \tag{40}$$

Denoting the last term in Eq. (40) with F_M and substituting there F in the form of the series Eq. (18), one obtains

$$F_M \equiv \frac{1}{M}\left(\sum_{m=0}^{M-1} \mathcal{K}^m Q + \sum_{m=1}^{M} \mathcal{K}^m F\right) = \sum_{k=0}^{\infty} \mathcal{K}^k Q_M, \tag{41}$$

which is a series solution to Eq. (36).

Equation (36) describes one iteration of the solution procedure which results in

$$F = \sum_{i=1}^{\infty} \Delta F_M^{(i)}, \quad \Delta F_M^{(i)} = \Delta F_M(Q^{(i)}), \tag{42}$$

with

$$Q^{(i)} = Q_M(Q^{(i-1)}), \quad Q^{(1)} = Q_t. \tag{43}$$

In accordance with Eq. (42), the averages are given by

$$D_{\text{mono}} = \lim_{N_{\text{it}}\to\infty} \sum_{i=1}^{N_{\text{it}}} D_{\text{mono}}^{(i)}, \quad \lambda_{bb} = \lim_{N_{\text{it}}\to\infty} \sum_{i=1}^{N_{\text{it}}} \lambda_{bb}^{(i)}, \tag{44}$$

where $D_{\text{mono}}^{(i)}$ and $\lambda_{bb}^{(i)}$ are given by Eqs. (4) and (5), respectively, with the substitution $\hat{f}=g^{-1/2}F_M^{(i)}$ there and N_{it} is the number of iterations. The first iteration is performed using a standard δf method advancing N test particles initially distributed according to Eq. (22) by $M-1$ steps so that each of them gains the (random) weight

$$W_{(M-1)} = \sum_{j=0}^{M-1} [1-\chi(\mathbf{z}_{(j)})]\dot{\psi}(\mathbf{z}_{(j)})\Delta t, \tag{45}$$

and the averages are estimated as an ensemble average,

$$D_{\text{mono}}^{(1)} \approx -\frac{1}{\langle|\nabla\psi|\rangle^2}\frac{1}{N}\sum_{\text{particles}} W_{(M-1)}\dot{\psi}(\mathbf{z}_{(M-1)}), \tag{46}$$

$$\lambda_{bb}^{(1)} \approx -\frac{3}{\rho_L B_0\langle|\nabla\psi|\rangle}\frac{1}{N}\sum_{\text{particles}} W_{(M-1)}\lambda_{(M-1)}B(\mathbf{z}_{(M-1)}). \tag{47}$$

Starting from the second iteration the algorithm with constant weights is used. For this purpose, in accordance with Eq. (37), the weight of each test particle is changed to $w=W_{(M-1)}/M$ where $W_{(M-1)}$ is its weight after the first iteration, and these particles are again advanced by $M-1$ steps with these fixed weights. During each such step their weights

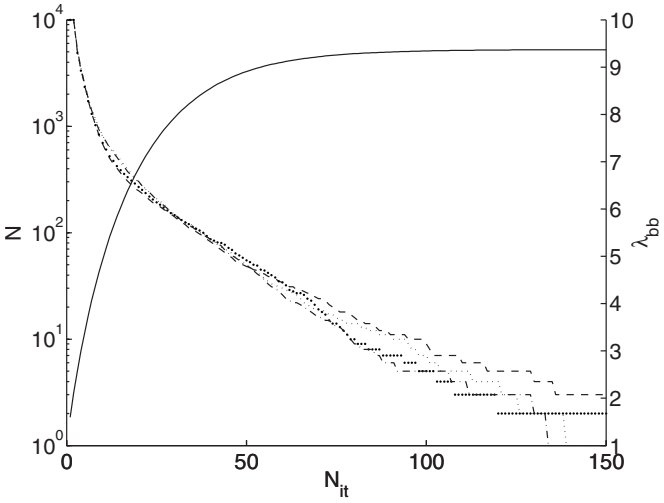

FIG. 3. Number of simulation particles N for four sub-runs (left axis, dashed lines) and final value of the bootstrap coefficient λ_{bb} computed from 40 sub-runs (right axis, solid line) vs number of iterations N_{it}. Here, 150 iterations approximately correspond to five collision times.

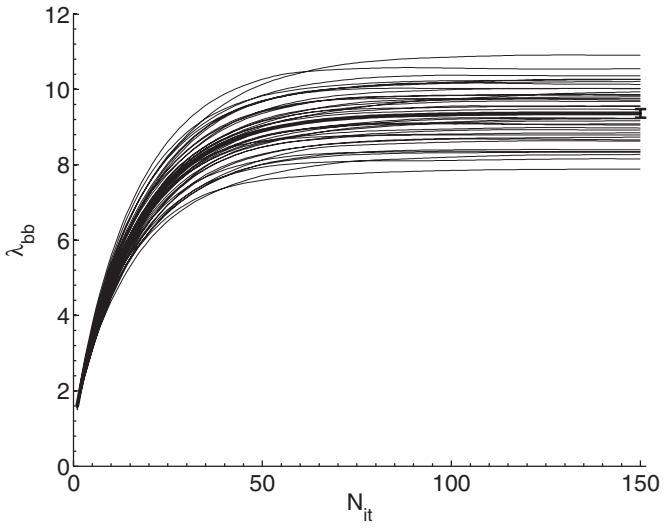

FIG. 4. Bootstrap coefficient λ_{bb} for a sample of sub-runs (thin lines), where $K=40$, and the average value (thick line) plotted over the number of iterations N_{it}. The estimated standard deviation σ_K of the final value is shown with an error bar.

are counted on the 3D grid in phase space producing in this way a source term $Q^{(3)}$ for the next iteration while the contribution to the averages is computed directly as

$$D^{(i)}_{\text{mono}} \approx -\frac{1}{\langle|\nabla\psi|\rangle^2}\frac{1}{N}\sum_{\text{particles}} w\sum_{k=0}^{M-1}\dot{\psi}(\mathbf{z}_{(k)}), \tag{48}$$

$$\lambda^{(i)}_{bb} \approx -\frac{3}{\rho_L B_0\langle|\nabla\psi|\rangle}\frac{1}{N}\sum_{\text{particles}} w\sum_{k=0}^{M-1}\lambda_{(k)}B(\mathbf{z}_{(k)}), \tag{49}$$

where $i=2$ and starting positions $\mathbf{z}_{(0)}$ are the final positions $\mathbf{z}_{(M-1)}$ of the first iteration. Finally, for the third and all further iterations test particles are generated from the source determined on the grid. Namely, in accordance with Eq. (37), the weight scored in each grid cell during a previous iteration is divided by M thus giving w_{cell}. Then test particles with a prescribed weight modulus $w_{(0)}$ are generated in grid cell centers with a probability proportional to $|w_{\text{cell}}|/w_{(0)}$ and signs of their weights w given by the sign of the pertinent w_{cell}. The prescribed weight $w_{(0)}$ is different in the "trapped" and "passing" regions of the phase space separated by a splitting boundary as shown in Fig. 2. These weights are prescribed after the second iteration as

$$w^t_{(0)} = \frac{1}{N}\sum_{\text{cells}}|w_{\text{cell}}|, \quad w^p_{(0)} = w^t_{(0)}/n_{\text{split}}, \tag{50}$$

where t denotes trapped, p denotes passing, and n_{split} is chosen in order to make the number of test particles in both phase space regions roughly the same. In the long mean free path regime, the weight contained in the "trapped" region is large compared to the weight in the "passing" region. In addition, test particles with $w^t_{(0)}$ which cross the splitting boundary and enter the passing region during the iteration are also split into n_{split} particles. Since prescribed weights stay further unchanged, the total number of test particles is decreasing with iterations due to annihilation of their weights on the grid (see Fig. 3). Despite the decreasing number of test particles, contributions to the averages from iterations $i \geqslant 3$ are also determined by Eqs. (48) and (49) with the same value of N as for the first iteration.

The number of steps M for a single iteration is chosen to be much smaller than collision time and large enough in order to fill the grid using a limited number of test particles. Since the filtering (limitation of test particle motion by the annulus) is not used in the procedure described above, the main source of the bias besides the negligible small error in the Monte Carlo operator may come from the rediscretization procedure. In order to keep this error within predefined limits, a rather large size of the grid over ϑ and φ was chosen, 100×100, while the size of the grid over the pitch parameter λ is chosen so that the grid cell width over λ is smaller with a certain tolerance than the diffusive change in pitch after a rediscretization time $iM\Delta t$. Iterations are continued until no particles are left for the next iteration. Typically, this corresponds to $iM\Delta t$ equal to a few collision times (see Fig. 3). At this point the result is fully converged, the convergence with iteration number is exponential.

IV. COMPUTATIONAL RESULTS

For numerical computations the code NEO-MC has been developed. In order to speed up the computations the batch system Condor is used which allows to run subsets of particles on different CPUs at the same time. Typically $N=10^4$ particles are started in a single subset. Each of these K subruns delivers results for the transport coefficients which have to be joined appropriately to get the final value (see Fig. 4). The results of the sub-runs are used to estimate the variance of these final values according to

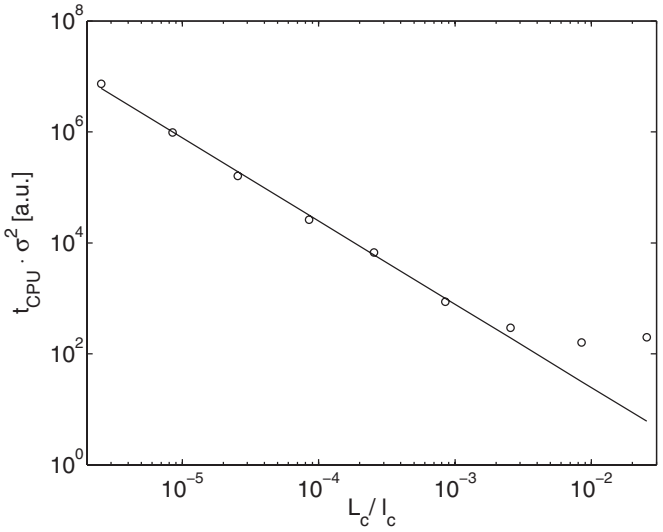

FIG. 5. CPU time multiplied with the variance of the bootstrap coefficient σ^2 plotted over the collisionality parameter (○). The solid line shows the scaling $(l_c/L_c)^{3/2}$.

$$\sigma_K^2 \approx \frac{1}{K-1}\sum_{k=1}^{K}(A_k - \langle A\rangle_K)^2, \tag{51}$$

where A_k are the results computed by the individual sub-runs and σ_K is the standard deviation of the average over sub-runs

$$\langle A\rangle_K = \frac{1}{K}\sum_{k=1}^{K} A_k. \tag{52}$$

In Fig. 3 together with the number of test particles the sum entering the limit for λ_{bb} in Eq. (44) is plotted over the number of iterations N_{it} for a couple of sub-runs. The change of each λ_{bb} value towards the end of the computation is small due to the fact that at the end of the integration path there are only few test particles remaining which deliver contributions to λ_{bb}.

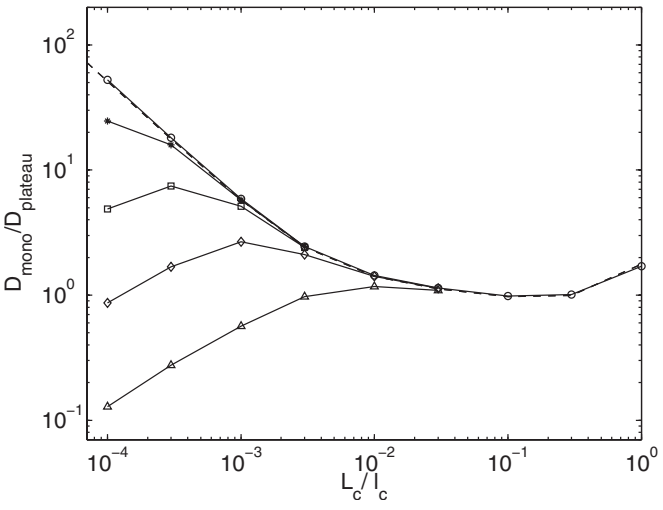

FIG. 6. Normalized diffusion coefficient $D_{\text{mono}}/D_{\text{plateau}}$ for LHD with $R=375$ cm vs collisionality parameter L_c/l_c at half plasma radius computed by NEO-MC (solid lines) and NEO-2 (dashed line) for $E_r/(vB)=0$ (○), 3×10^{-5} (*), 1×10^{-4} (□), 3×10^{-4} (◇), 1×10^{-3} (△).

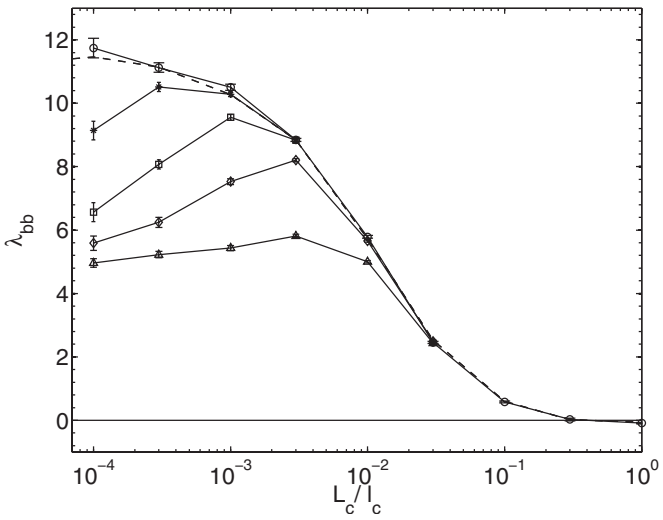

FIG. 7. Normalized bootstrap coefficient λ_{bb} for LHD with $R=375$ cm vs collisionality parameter L_c/l_c at half plasma radius. Markers and line types are the same as in Fig. 6.

As a result of the described improvements of the δf method, the variance of this method is reduced to the scaling l_c/L_c as compared to the scaling $(l_c/L_c)^2$ of the standard δf method without filtering for the same number of test particles N at the start of the computation. In addition, due to the decay of test particle numbers with iterations, the CPU time needed for the same number of starting particles is also reduced from the usual linear scaling, l_c/L_c, to the scaling $(l_c/L_c)^{1/2}$. As a result, the CPU time needed to achieve a given accuracy by the improved method scales as $(l_c/L_c)^{3/2}$. This can be seen from Fig. 5 where normalized run times are shown as functions of collisionality L_c/l_c. The deviations at the higher collisionalities from the expected scaling are caused by the time needed for the precomputation of the magnetic field data which makes up the major part of the total computation time there. For low collisionalities this precomputation time is negligible compared to the time needed

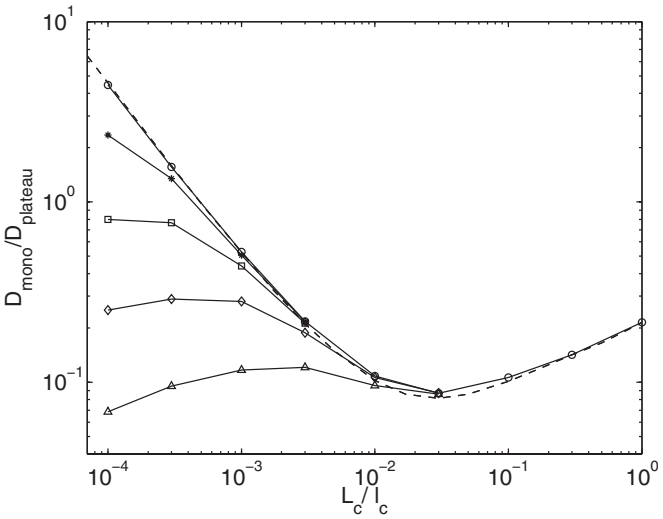

FIG. 8. Normalized diffusion coefficient $D_{\text{mono}}/D_{\text{plateau}}$ for W7-X standard configuration vs collisionality parameter L_c/l_c at half plasma radius. Markers and line types are the same as in Fig. 6.

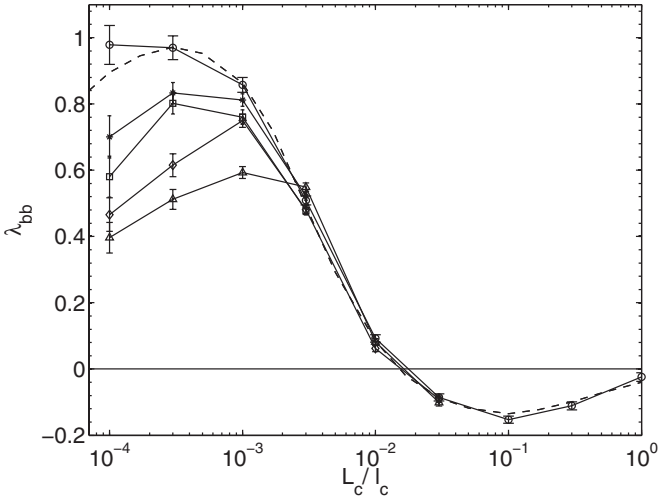

FIG. 9. Normalized bootstrap coefficient λ_{bb} for W7-X standard configuration vs collisionality parameter L_c/l_c at half plasma radius. Markers and line types are the same as in Fig. 6.

for running the particles. Such a scaling is much better than the scaling $(l_c/L_c)^3$ of the standard δf method without a filter.

It should be noted, that from the viewpoint of rediscretization it would be most effective to start all particles in a single run instead of distributing them to subsets, but from a practical point of view the usage of a computer cluster as for the computations in this paper is advantageous for the total computing times as well as for estimation of variances.

Results of computations with negligible radial electric fields for the LHD-375 configuration[8] and the W7-X standard configuration[9] stay in good agreement with results of NEO-2, a field line tracing code which computes transport coefficients for zero radial electric fields in arbitrary collisionality regimes,[10] as shown in Figs. 6–9. There, 80 subruns have been used for the computations. First results of benchmarking of the computations with finite radial electric fields with other methods can be found in Ref. 11. Those results also stay in good agreement with, e.g., DKES[12] computations.

V. SUMMARY

In this paper, an improved δf Monte Carlo method has been developed for computation of monoenergetic neoclassical transport coefficients in stellarators. This method uses a rediscretization procedure and importance sampling in order to reduce the variance of these coefficients. As a result, the CPU time required for given accuracy of the computation of the bootstrap coefficient scales as a mean free path in power of 3/2. The bias introduced by this method can be limited to very low values with small cost in terms of CPU time. In addition, the method allows simultaneous computation of the bootstrap coefficient and the diffusion coefficient. The computer code using this method has been benchmarked with computations by other methods and stays in good agreement with those results.

ACKNOWLEDGMENTS

This work, supported by the European Communities under the contract of Association between EURATOM and the Austrian Academy of Sciences, was carried out within the framework of the European Fusion Development Agreement. The views and opinions expressed herein do not necessarily reflect those of the European Commission. Additional funding is provided by the Austrian Science Foundation, FWF, under Contract No. P16797-N08.

[1] M. Sasinowski and A. H. Boozer, Phys. Plasmas **2**, 610 (1995).
[2] M. Sasinowski and A. H. Boozer, Phys. Plasmas **4**, 3509 (1997).
[3] W. X. Wang, N. Nakajima, M. Okamoto, and S. Murakami, Plasma Phys. Controlled Fusion **41**, 1091 (1999).
[4] J. D. Williams and A. H. Boozer, Phys. Plasmas **10**, 103 (2003).
[5] M. Yu. Isaev, S. Brunner, W. A. Cooper, T. M. Tran, A. Bergmann, C. D. Beidler, J. Geiger, H. Maassberg, J. Nührenberg, and M. Schmidt, Fusion Sci. Technol. **50**, 440 (2006).
[6] K. Allmaier, S. V. Kasilov, W. Kernbichler, G. O. Leitold, and V. V. Nemov, in *34th EPS Conference on Plasma Physics, Warsaw, Poland, 2–6 July 2007*, edited by P. Gasior and J. Wołowski (European Physical Society, Mulhouse, 2007), ECA Vol. 31F, P-4.041.
[7] A. H. Boozer and G. Kuo-Petravic, Phys. Fluids **24**, 851 (1981).
[8] S. Murakami, A. Wakasa, H. Maaßberg, C. D. Beidler, and H. Yamada, Nucl. Fusion **42**, L19 (2002).
[9] H. Maassberg, W. Lotz, and J. Nührenberg, Phys. Fluids B **5**, 3728 (1993).
[10] W. Kernbichler, S. V. Kasilov, G. O. Leitold, V. V. Nemov, and K. Allmaier, in *33rd EPS Conference on Plasma Physics, Rome, Italy, 19–23 June 2006*, edited by F. De Marco and G. Vlad (European Physical Society, Mulhouse, 2006), ECA Vol. 30I, P-2.189 (2006).
[11] K. Allmaier, C. D. Beidler, M. Yu. Isaev, S. V. Kasilov, W. Kernbichler, H. Maassberg, S. Murakami, D. A. Spong, and V. Tribaldos, in *16th International Stellarator/Heliotron Workshop 2007, Toki, Japan, 15–19 October, 2007*, edited by S. Morita (National Institute for Fusion Science, Toki, 2008), NIFS-PROC-69, P2-029.
[12] W. I. van Rij and S. P. Hirshman, Phys. Fluids B **1**, 563 (1989).